crystals

MDPI

Article

High-Temperature Evolution of the Incommensurate Composite Crystal $Ca_{0.83}CuO_2$

Lara Righi [1,2,*], Marco Merlini [3] and Mauro Gemmi [4]

1 Department of Chemistry, Life Sciences and Environmental Sustainability, University of Parma, Parco Area delle Scienze 17/A, 43124 Parma, Italy
2 IMEM-CNR, Parco Area delle Scienze 37/A, 43124 Parma, Italy
3 Department of Earth Sciences "Ardito Desio", University of Milan, Via Mangiagalli, 34 20133 Milan, Italy; marco.merlini@unimi.it
4 Center for Nanotechnology Innovation @NEST, Istituto Italiano di Tecnologia, Piazza San Silvestro 12, 56127 Pisa, Italy; mauro.gemmi@iit.it
* Correspondence: lara.righi@unipr.it

Received: 1 July 2020; Accepted: 20 July 2020; Published: 21 July 2020

Abstract: The crystal structure of the composite crystal $Ca_{0.83}CuO_2$ was investigated by synchrotron powder diffraction at high temperature. The incommensurate modulated structure was firstly analyzed at room temperature (RT) and successfully solved by adopting the (3D + 1)-dimensional symmetry $P2_1/m(\alpha 0 \gamma)0s$. The composite crystal is featured by a non-uniform distribution of Ca ions occupying octahedral sites formed by the spatial arrangement by the infinite 1D CuO_2 chains. By approaching 500 K, $Ca_{0.83}CuO_2$ undergoes a structural rearrangement ruled by the shrinking of the Ca interatomic distances. The high-temperature crystalline phase is characterized by a different incommensurate periodicity requiring the recombination of the Ca/CuO_2 balance featuring the composite intergrowth of the two almost independent sub-structures. We ascertain that the new crystalline form is stable up to 950 K near to the limit of the thermal decomposition.

Keywords: composite crystals; Ca-based cuprates; incommensurate modulation; powder synchrotron diffraction study

1. Introduction

The study of the phase diagrams involving copper oxide CuO and alkaline or alkaline earth oxides demonstrated the occurrence of phases characterized by common structural features with general formula A_xCuO_2, where typically x = 1 for A = Na, K and 0.67 < x < 0.90 for A = Ca, Sr, Ba. Alkaline-based cuprates, like $NaCuO_2$ and $KCuO_2$, consist of alkaline layers [1–4] interpenetrated by edge-sharing CuO_2 ladders. The different size of Na and K cations, rules the periodic arrangement CuO_2 stripes and cations. Octahedral sites, formed by oxygen atoms of adjacent CuO_2 chains, are occupied by the alkaline cations in a 1:1 ratio with the CuO_2 units. For A = Ca^{2+}, Sr^{2+} or Ba^{2+}, the structure remains strictly related to that of the corresponding alkaline-based compounds but, as a result of the increased atomic size, only a fraction of the octahedral sites is occupied and the compound results to be non-stoichiometric. Indeed, as the ionic radii of the alkaline-earth increases, A^{2+}/Cu decreases progressively as evidenced by the compositions reported in literature [5–8] and summarized in Table 1. The remarkable compositional flexibility is demonstrated by the occurrence of Na-based compounds with chemical composition $Na_{1.66}CuO_2$ showing a stable excess of Na^+ ions [9]. So far, K-based off-stoichiometric $K_{1.5}CuO_2$ can be efficiently fabricated [10], being the inferior content of K likely ascribable to the similar correlation between ionic radii and chemical composition observed for the alkaline-earth group of cuprates. Nevertheless, several structural studies accounted that this family of

cuprates represent a prototypical example of composite crystal [11–13]. Indeed, the crystalline phase is composed of two distinct sub-structures associated to the A cations and CuO_2 symmetries, respectively. The different symmetry and periodicity of the two sub-systems give rise to incommensurate displacive modulation observed in all the off-stoichiometric compounds [9,10,14–18]. The mismatch of the two sub-units, ruling the A/Cu balance, is generally confined to a single fundamental periodicity giving rise to a mono-dimensional incommensurate modulation.

Table 1. Correlation between stoichiometry of A_xCuO_2 and ionic dimension of alkaline-earth cations.

A	x	Effective Ionic Radii (r_e)
Ca^{2+}	0.83–0.85	1.00
Sr^{2+}	0.73	1.18
Ba^{2+}	0.67–0.70	1.35

It is worth to recall that, similarly to the Cu-based family, a series of 1D layered compounds showing similar incommensurate modulated structure was discovered for alkaline and alkaline-earth cobalt oxides [19,20]. The layered $Na_{0.83}CoO_2$ composite crystal crystalizes in a triclinic symmetry and possess interesting thermoelectric properties [20].

The occurrence of infinite edge-sharing CuO_2 chains is a structural character of few materials and a series of unusual physical and chemical properties are featuring this family of compounds. Ordered mono-dimensional 1D spin arrangement was found in the $SrCu_2O_3$ and $Sr_{14}Cu_{24}O_{41}$ compounds [21–23]. The antiferromagnetic (AFM) ordering observed in $Sr_{14}Cu_{24}O_{41}$ below 60 K has been related to the spin orientation predominantly perpendicular to the 1D CuO_2 chains [22]. This is confirmed by the observation of similar antiferromagnetic coupling in $Sr_{0.73}CuO_2$ [5,24], below 10 K. Analogously, incommensurately modulated calcium cuprates are characterized at low temperature by AFM coupling [17]. The magnetic properties of such cuprates show a complex behavior associated to the interplay of different 1D spin configurations (spin dimers, alternating Heisemberg chains, etc.). The off-stoichiometry is compensated by hole-doping of the cuprate ribbons with the proper balance of Cu^{2+}/Cu^{3+} ratio. Interestingly, the Cu valence is not randomly distributed, but it is observed charge ordering giving rise to periodic magnetic correlations [25]. Recent inelastic neutron scattering studies on $(Ca,Y)_{0.82}CuO_2$ disclosed complex ferromagnetic frustrated interactions involving adjacent CuO_2 chains having a mono-dimensional (1D) AFM ordering [26].

Nevertheless, the $Ca_{0.83}CuO_2$ system exhibits a remarkable activity in the catalytic oxidation of volatile organic compounds, as well as the unusual ability to adsorb gases such as NOx, CO, CO_2, with strong selectivity toward NO_x [27]. The reversibility of the sorption process, induced by thermal treatments, could make Ca_xCuO_2 with $0.824< x <0.84$ a suitable material for de-NOx applications [27,28]. Furthermore, Ca-based cuprates gathered increasing attention in the field of nanocatalysis for the synthesis of different aromatic aldehydes, in solvent-free modes [29]. These novel applications demand the knowledge of the structural properties at the high-temperature regime suitable for catalytic and gas up-taking applications. Up to now, the structural studies of the off-stoichiometric cuprates was dedicated to the low temperature properties. In this work we present valuable insights obtained by the structural analysis of the $Ca_{0.83}CuO_2$ compound carried out by increasing the temperature up to 1073 K. The detailed structure determination of such complex incommensurate composite crystal was successfully achieved by introducing the superspace approach [13]. The experiments were performed adopting a time-resolved mode with a Debye–Scherrer diffractometer implemented in the BM08 beamline of ESRF large facility. The Rietveld refinements performed on the powder diffraction data unveil the complex evolution of the $Ca_{0.83}CuO_2$ composite crystal at high-temperature conditions.

2. Materials and Methods

$Ca_{0.83}CuO_2$ samples have been prepared following the technique of pyrolysis of a gel obtained from an acid solution of citrates of Cu and Ca metals. The starting reagents $CaCO_3$ and CuO are

dissolved by a concentrated solution of HNO_3. Afterwards, an excess of citric acid to the solution is added in order to form agglomerates with Ca and Cu metals. The prepared solution is then heated to remove water in order to obtain a colored blue gel. The further heating of the gel results in a pyrolysis where the organic components are removed. The final reactive amorphous powder is treated at 700 °C under flowing oxygen. Powder diffraction X-ray collected with a X'TRA diffractometer (Thermo Fisher, Switzerland) using a CuKα radiation, confirmed the successful synthesis of the cuprate excluding the presence of secondary phases. A high-resolution diffraction pattern collected with a low counting rate was used to perform the first structure refinement. The obtained crystallographic model was then adopted for the high-temperature structural investigation. Moreover, transmission electron microscopy (TEM) study was carried out with a Philips CM30T microscope (Philips, Germany) operating with 300 Kv. Electron diffraction (ED) patterns was collected using a Gatan slow-scan CCD camera (Philips, Germany).

The powder diffraction experiments were performed on the BM08 beamline at ESRF (European Synchrotron Radiation Facility, Grenoble, France) synchrotron with the radiation $\lambda = 0.685$ Å. A glass tube containing the sample was accommodated in a holder conveniently positioned over a gas blower heater. A translating imaging plate (IP) has been used to record the structural transition during the overall heating session. To couple the translating motion of the IP and the temperature change, a thermocouple was inserted in the vicinity of the polycrystalline sample. The integration of the diffraction patterns was carried out by defining time intervals corresponding to selected temperatures ranges (every 50 K). The heating system prevented a fine control of the temperature during the in-situ experiments, but we were able to collect diffraction patterns with suitable resolution in the range 400–950 K. The Rietveld refinements was undertaken with Jana2006 suite [30] by adopting the superspace approach [11–13].

3. Results and Discussion

In earlier works, ED and HREM investigations [14,15] addressed the structural study of Ca and Ba based cuprates. ED patterns manifest the typical features of composite crystals showing diffraction spots associated to two independent lattices. The indexing of the separated groups of the main reflections provided the following cell constants [15]:

(1) a = 2.80 Å, b = 6.32 Å, c = 10.57 Å (Orthorhombic Fmmm symmetry)
(2) a = 3.36 Å, b = 6.32 Å, c = 5.47 Å, $\beta = 104.9°$ (Monoclinic C2/m symmetry)

The former is consistent with the typical arrangement of copper-oxygen chains in A_xCuO_2 compounds [14–16] and it is readily assigned to CuO_2 sublattice, the latter being clearly related to Ca sub-lattice periodicity. This interpretation agrees with the ED study that we performed on the samples fabricated and used for the high-temperature diffraction experiments. The indexing of spots observed in ED data by using Ca and CuO_2 reciprocal lattices is presented in the Supplementary Material Figure S1. As it is illustrated in the Figure 1, the composite crystal $Ca_{0.83}CuO_2$ is formed by the interpenetrating of the distinct lattices with their own translational symmetry. When the ratio of the unit cell volumes of the two sublattices is irrational, the two sub-structures coexist with off-stoichiometric compositions. The mutual interaction of Ca layers and CuO_2 ribbons is accompanied by structural modulation. As a result, the diffraction pattern of a composite crystal is the superimposition of the diffraction patterns of the two sublattices and satellite reflections. In the frame of the superspace approach the (3D + 1)-dimensional structure of a composite crystal, the first sub-unit is associated to the *hkl0* indices, while the indices of the second one are given by *0klm* with a shared reciprocal plane with indices *0kl0*. Reflections *hklm* are the result of the mutual interaction of the two subsystems. The whole ED pattern is indexed by adopting the diffraction vector:

$$\mathbf{H} = h\mathbf{a}^* + k\mathbf{b}^* + l\mathbf{c}^* + m\mathbf{q} \quad (1)$$

where **a***, **b*** and **c*** are related to one sub-lattice, whereas the modulation vector **q** = α**a*** + β**b*** + γ**c*** represents the incommensurate periodicity of the second sub-lattice. The incommensurate crystal structure of $Ca_{0.83}CuO_2$ was solved by Miyazaki et al. [17] on the basis of both x-ray and neutron powder diffraction data. The composite crystal was represented by assigning the non-conventional space group F2/m(1 + α 0 γ)0s with a modulation vector assuming the form **q** = x $\mathbf{a}^*_{CuO2}$ + (1 − x)$\mathbf{c}^*_{CuO2}$. Indeed, the authors converted the monoclinic Ca sub-lattice by adapting a F centered cell with the following constants: a = 3.36 Å, b = 6.32 Å, c = 10.59 Å, β = 92.99°. This model represents the first application of the superspace formalism to the structure description of the $Ca_{0.83}CuO_2$ incommensurate composite crystal at room temperature [17]. In the actual work, we define the composite crystal with a different approach based on the monoclinic lattice associated to the Ca lattice. This new setting is illustrated in Figure 1 wherein both CuO_2 and Ca sub-units are referred to a monoclinic symmetry having the **c** constant coinciding with 5.47 Å, but with different monoclinic angle.

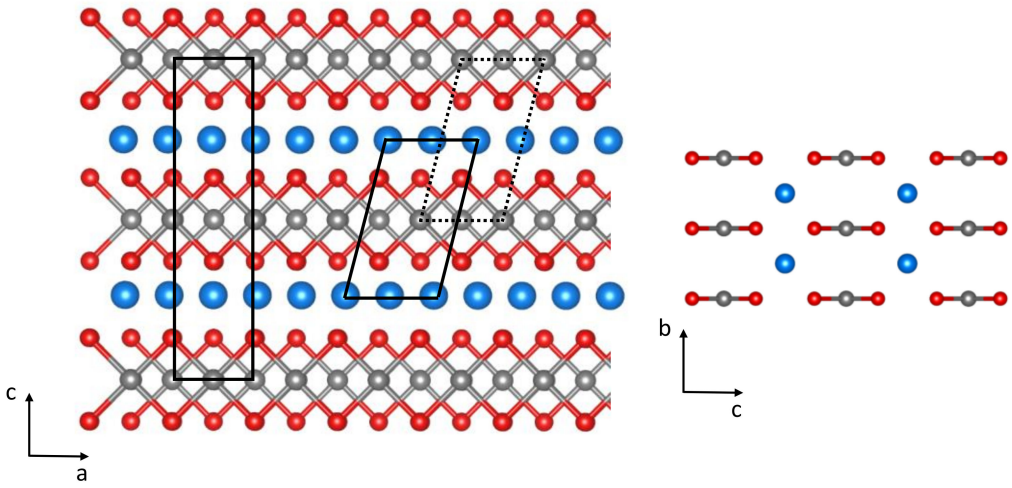

(**a**) (**b**)

Figure 1. (**a**) Ideal model of the undistorted structure of $CaCuO_2$. The colors correspond to: Ca-blue, Cu-gray and O-red. The projected CuO_2 edge-shared chains are shifted of $\frac{1}{2}$ along the **a** axis. The F-centered and monoclinic lattices are indicated with black lines for CuO_2 and Ca sub-structures respectively. The dashed lattice represents the CuO_2 unit cell projection in the monoclinic composite crystal adopted in the actual study. (**b**) View of the ideal model along the fundamental **a** axis.

The base reciprocal vectors for the composite structure are correlated by the (3 + 1)-dimensional matrix:

$$\begin{bmatrix} a^*_{Ca} \\ b^*_{Ca} \\ c^*_{Ca} \\ q_2 \end{bmatrix} = \begin{bmatrix} 0 & 0 & 0 & 1 \\ 0 & 1 & 0 & 0 \\ 0 & 0 & 1 & 0 \\ 1 & 0 & 0 & 0 \end{bmatrix} \begin{bmatrix} a^*_{CuO2} \\ b^*_{CuO2} \\ c^*_{CuO2} \\ q_1 \end{bmatrix}$$

In this frame, the superspace symmetry for the CuO_2 sub-structure is $P2_1/m(\alpha 0)0s$, characterized by non-primitive translation conforming the m_s mirror. The symmetry rules define the modulation vector as **q**= α**a*** + γ**c*** having α equivalent to both the x compositional parameter Ca_xCuO_2 and the a_{CuO2}/a_{Ca} fraction [14,15]. The fundamental undistorted structure of CuO_2 is constituted by a special position for Cu and two independent positions for O with coordinates (x, $\frac{1}{4}$, z). The Ca atom is positioned at the origin of the second basic sub-structure. The modulation of the three atomic species was defined by the Fourier modulation function:

$$u^i(\bar{x}_4) = \sum_{n=1,2} A^i_n \sin(2\pi n \bar{x}_4) + B^i_n \cos(2\pi n \bar{x}_4) \quad (2)$$

where x_4 represents the four-dimensional variable in the superspace, and the A^i and B^i parameters allowed by the symmetry are refined to determine the displacive modulation for each atomic site. To finely describe the modulation function of the atomic species, we introduced the first and second order of the cosine and sine components of the Fourier series.

The (3D + 1)-dimensional crystal data of the Rietveld refinement obtained from the RT diffraction data are summarized in the Table 2. The structural refinement achieved the agreement factors R_p = 2.26% R_{wp} = 3.07% and the Rietveld output plot is depicted in Supplementary Material Figure S2. The refined modulation vector **q** = 0.83057(7)**a*** + 0.0032(3)**c*** agrees with the nominal chemical composition. The a_{CuO2} cell constant can be related to a_{Ca} with the simple relation $6a_{CuO2} = 5a_{Ca}$, from which $a_{CuO2}/a_{Ca} = 5/6 = 0.833$, therefore, the chemical formula could be suitably indicated as $Ca_5Cu_6O_{12}$.

Table 2. Summarized crystal data for the (3D + 1)-dimensional crystal structure of $Ca_{0.83}CuO_2$ composite crystal at RT.

	Sublattice CuO_2	**Sublattice Ca**
Space Group	$P2_1/m(\alpha 0 \gamma)0s$	$P2_1/a(\alpha 0 \gamma)00$
Crystal system	Monoclinic	Monoclinic
Unit Cell (Å,°)	a = 2.8010(5)	a = 3.3277(5)
	b = 6.3193(1)	b = 6.3193(1)
	b = 5.4734(9)	c = 5.4734(9)
	β = 104.939(4)	β = 105.040(4)
q	0.83057(7)a* + 0.0032(2)c*	1.20144(7)a* - 0.0038(6)*c
Atomic position (x, y, z)	Cu1 $\frac{1}{4}$ $\frac{1}{4}$ $\frac{1}{4}$	Ca1 0 0 0
	O1 0.625(4) $\frac{1}{4}$ 0.252(2)	
	O2 0.875(5) $\frac{1}{4}$ 0.741(2)	
Isotropic ADP	Cu1 0.021(10)	Ca1 0.101(90)
U_{iso} (Å^2)	O1 0.033(32)	
	O2 0.025(35)	
Global R indexes	R R_w	
Main Reflections	0.0187 0.0162	
Composite part Ca	0.0152 0.0147	
Composite part CuO_2	0.0232 0.0194	
R_p	0.0226	
R_{wp}	0.0307	

Table S1 resumes the refined values of the A^i and B^i amplitudes associated to the fractional basic coordinates. Concerning the Cu-O interactions, the four-fold coordination is far from the ideal planar configuration being perturbed by the propagation of a tilted wave along the ribbons. The Cu-O distances are characterized by an oscillating mean bond length ranging from 2.05 to 1.85 Å with a global average of 1.93 Å. The distortion of the CuO_2 chains is related to the periodic charge ordering well described by plotting the modulated Cu-O lengths calculated from the (3D + 1)-dimensional model. The sequence of the in-phase shrinkages and expansions of the square coordination can be correlated with the mixed valence Cu^{2+}/Cu^{3+}. The bond valence (BV) plot of Figure 2c demonstrates that the Cu oxidation alternates between 2+ and 3+ limits, with the same period of Cu-O modulated interactions. The assigned valence must be interpreted bearing in mind that, for such a complex structure, the bond valence evaluation is not straightforward. Therefore, the upper region of the curve approaching 2.9 value was attributed to 3+ valence, whereas the region of the curve ranging from 1.8 to 2.2 likely corresponds to Cu^{2+}.

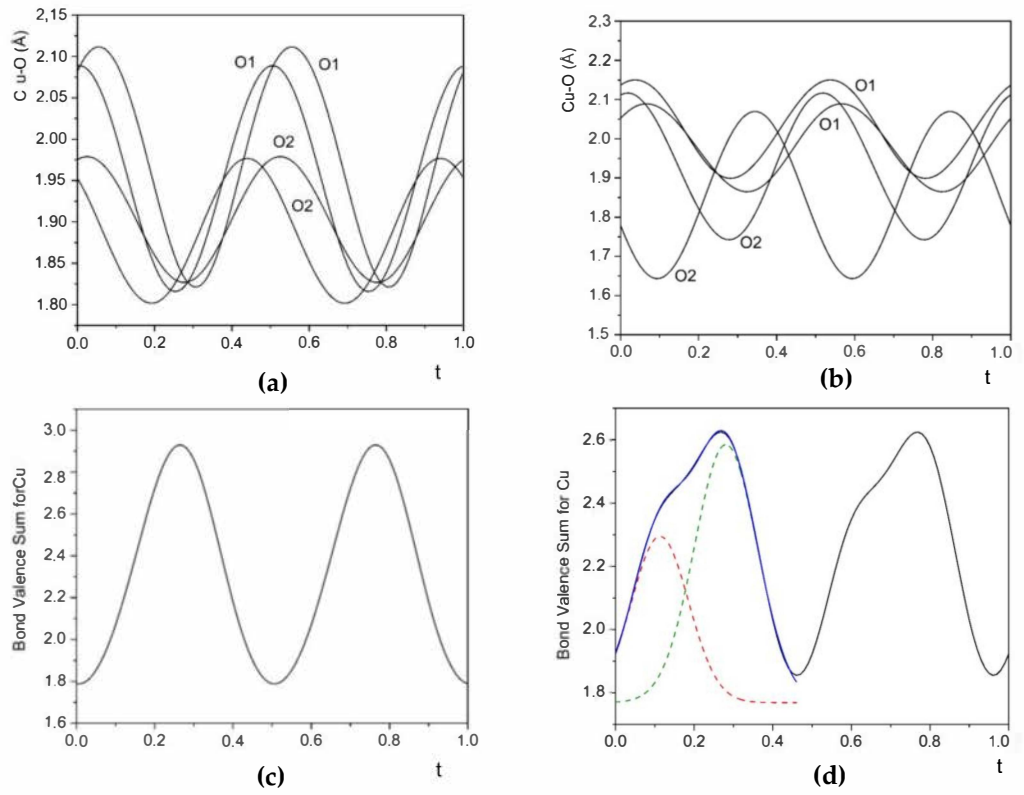

Figure 2. (**a**,**b**) Modulated Cu-O interactions versus internal incommensurate parameter t = x_4 - q·xi for RT and 890 K structures respectively. (**c**,**d**) BV summation obtained on the basis of the modulated Cu-O interactions for RT (**c**) and 890 K (**d**) phases. The red and green dotted curves represent gaussian functions used to fit the VB profile whilst the blue line corresponds to their convolution.

As a result, considering a commensurate six-fold periodicity, the CuO_2 chains are constituted by the sequence Cu^{2+}-Cu^{2+}-Cu^{3+}-Cu^{2+}-Cu^{2+}-Cu^{3+}. This charge ordering topology is in agreement with the spin hole arrangement formulated by M. Isobe at al. [18] for the $Ca_{0.824}CuO_2$ composition and with former studies treating the $Ca_{0.83}CuO_2$ magnetic properties [14–16].

Nevertheless, the wave-like modulation of oxygen sites determines the major distortions of the environment of Ca atoms with the occurrence of remarkably distorted octahedral sites (see Figure 3). In this sense, the mutual interplay of the two sub-units is essentially ruled by the displacive modulation of the oxygen sites.

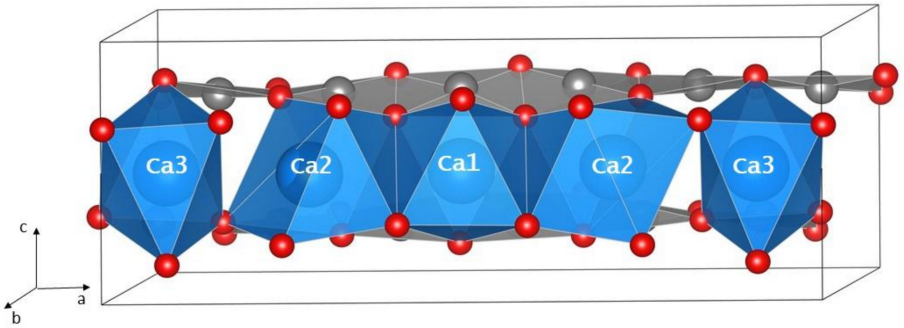

Figure 3. Commensurate superstructure for $Ca_5Cu_6O_{12}$. The graphical representation emphasizes the sequence of the three octahedral sites occupied by Ca^{2+}.

The hypersection of the (3D + 1)-dimensional composite crystal [11] corresponding to **q** = 5/6**a*** (the γ is approximated to 0 value) provides a commensurate superstructure having unit cell constants

$a = 6a_{CuO2} = 5a_{Ca}$, $b = b_{Ca}$, $c = c_{Ca}$ and $\beta = 104.9°$ with $P2_1/a$ symmetry (the crystal data are reported in the Table S2). The structure model consists of three independent positions for Cu and Ca atoms, having general coordinates $(x,\frac{1}{4},\frac{1}{2})$ and (x,0,0), respectively, and 6 sites for the oxygen atoms. The Figure 3 represents the commensurate five-fold superstructure where the Ca octahedral coordination and structural modulation of CuO_2 stripes are emphasized.

The sequence of edge-shared octahedra occupied by Ca^{2+} is discontinuous and after the third occupied site, the successive ideal Ca site is vacant. This cluster is represented in the Figure 3 by the Ca2-Ca1-Ca2 labelling being the Ca2 site markedly distorted. The next two octahedral sites indicated as Ca3 are rotated of about 90° with respect the previous orientation. The Ca2 coordination is affected by a strong deviation from the regular octahedral condition with at least 7 Ca-O short interactions ranging around 2.08 Å.

The high-temperature trend recorded in synchrotron diffraction experiments highlights the almost independent thermal expansion of the two sub-structures constituting the composite crystal.

In the Supplementary Material Figure S3, the overlay of the diffraction patterns collected in the temperature range 320–950 K is shown. Interestingly, the reflections associated to Ca sub-lattice are progressively shifted towards high 2θ region as the temperature increases. For each temperature step, Rietveld refinements was undertaken. The monoclinic model with $P2_1/m(\alpha 0 \gamma)0s$ is adopted for the overall temperature range and no change of symmetry of the (3D + 1)-structure was observed as it is indicated by the good agreement factors achieved for Rietveld refinements carried out for the high-temperature diffraction patterns (as an example see Supplementary Material Figure S4). The Figure 4 illustrates the evolution of the unit cell constants for both sub-lattices and corresponding change of the **q** vector against temperature. Upon heating, the composite crystal undergoes an adaptive structural change featured by the shrinking of Ca sub-structure. The onset of this structural transition corresponds approximately to 540 K as it is well drawn by the change of the **q** vector periodicity as well as the evolution of the **a** lattice parameter for both sub-structures (see Figure 4 a,b). Conversely, as it is illustrated also by the Figure 4d, by increasing the temperature, the CuO_2 sub-unit expands as expected. Beyond 500 K, the α parameter of the **q** modulation vector exhibits a marked increment moving from 0.830 to 0.851; the γ component abruptly increases and relaxes beyond 700 K. The deviation from a commensurate 5/6 periodicity indicates a recombination of the compositional Ca/Cu ratio mediated by the oxygen modulation. This is particularly evident by plotting the Cu-O lengths calculated for the 890 K structure wherein the structural recombination of the Ca-O interactions impacts on the CuO_2 chains. The Figure 2b shows that the Cu-O modulated lengths are spanned in a broad range and the Cu environment departs from the periodic alternation of short/long interactions observed in the phase stable at RT. The BV evaluation reported in the Figure 2d indicates a complex distribution of the mixed valence 2+/3+ for Cu and the calculated curve is actually the convolution of two periodic wave-like periodicities. The additional curve introduced to fit the BV profile shows a maximal value around 2.3 and the convolution of the two calculated Gaussian profiles point out a consistent rising of the Cu^{2+} content.

The average valence for Cu, extended throughout the incommensurate composite crystal, is around 2.28 with a slight but not negligible decrement with respect the oxidation state of 2.35 observed at room temperature. The shortening of the Ca-Ca distances rises the positive charge density in Ca_xCuO_2 compound which is, in turn, compensated by a decrease of Cu^{3+} occupancy alongside CuO_2 ribbons. The complex curve of the BV summation can be also interpreted by recalling earlier studies related to the synthesis of such compound under unconventional conditions [31,32].

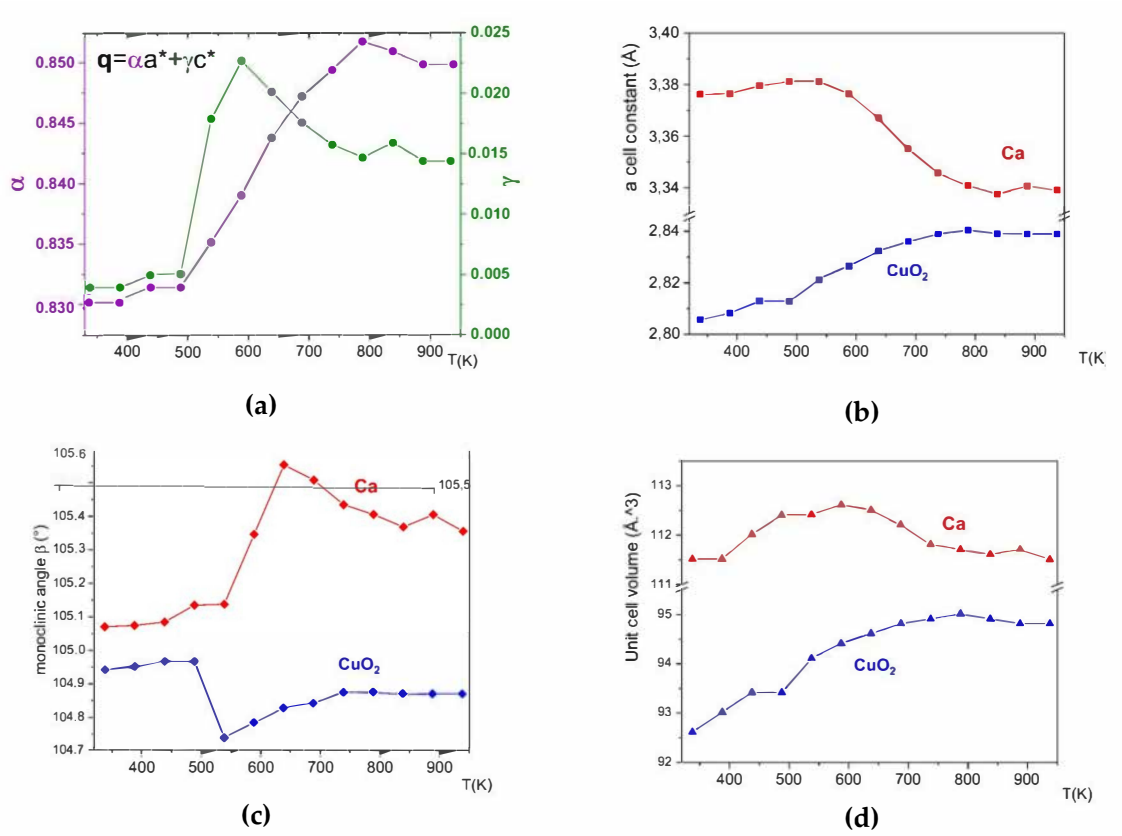

Figure 4. (**a**–**d**). Temperature dependence of the structural parameters featuring the modulated composite crystal $Ca_{0.83}CuO_2$. The red symbol/line is referred to the structure parameters of the Ca sub-structure whereas the blue one indicates the trend for CuO_2 part. The dimension of the symbols exceeds to e.d.s. for the refined parameters.

In particular, X.M. Qin and co-authors [32] explored high-temperature and high-pressure conditions to ascertain the stability of the off-stoichiometry Ca_xCuO_2 compounds. They accounted that, by crossing 1028 K, $Ca_{0.85}CuO_2$ decomposes into Ca_2CuO_3 + CaO at ambient pressure. Indeed, the additional curve convoluted in the BV periodicity could be related to the compositional instability, indicating an incipient phase separation of CaO and consequent formation of Ca_2CuO_3. Nevertheless, we did not notice the occurrence of CaO phase in the synchrotron diffraction pattern collected at high-temperature limit. Considering the crystal structure at 890 K, it is possible to define a new commensurate superstructure based on the broad assumption that for $\mathbf{q} = 0.851\mathbf{a^*} + 0\mathbf{c^*} \approx 6/7a^*$ so as $6a_{Ca} \approx 7a_{CuO2}$. The six-fold superstructure corresponding to the ideal $Ca_6Cu_7O_{14}$ composition has a triclinic P-1 symmetry with seven independent sites for Cu and Ca, respectively (see Table S3). Two symmetrically special sites of Ca atoms are occupied only by half in order to preserve compositional requirements. It is worth to stress that the new chemical formula is consistent to the redistribution of Ca and Cu cations across the average composite matrix and cannot be intended as a substantial increment of Cu amount. Hence, the chemical content remains constant but with a different spatial distribution over the average unitary crystal volume. In the six-fold supercell, depicted in Figure 5, the main difference with respect the RT structure relies on the more regular octahedral environments hosting Ca^{2+} ions. Among the seven sites for Ca, only Ca6 is affected by a strong distortion of the oxygen coordination with the occurrence of 7 Ca-O short interactions. The Ca6 site can be thus associated to the Ca2 of the $Ca_5Cu_6O_{12}$ RT phase, but in the actual structure this complex environment involves only 1/7, rather than 1/3, of the occupied interstices. The CuO_2 ribbons show the wave-like distortion already observed at low temperature.

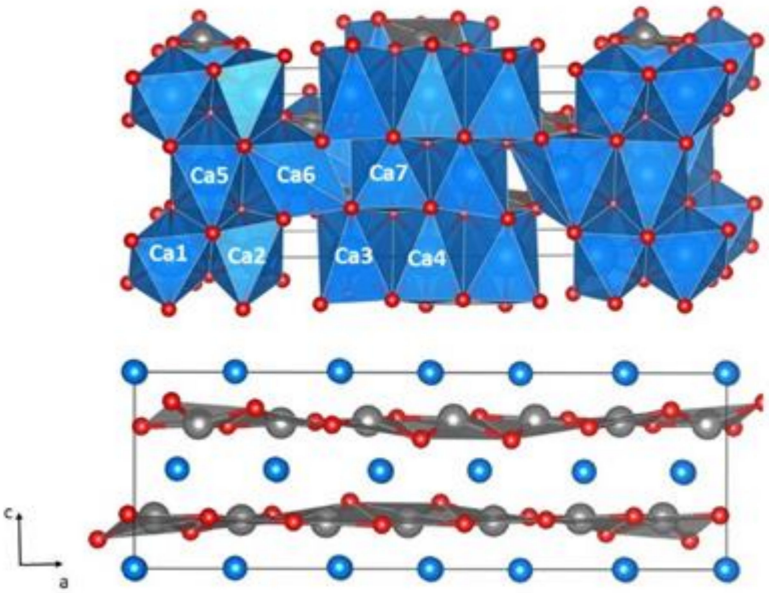

Figure 5. (**a**) Crystal structure of the high-temperature variant $Ca_6Cu_7O_{14}$. (**a**) Spatial distribution of the Ca^{2+}occupied sites. The Ca6 is affected by a strong deviation from typical octahedral geometry. (**b**) Displacive modulation of the CuO_2 ribbons. Note the out-of-plane distortion of Cu^{2+} square planar coordination.

4. Conclusions and Future Perspectives

The crystal structure of the composite crystal $Ca_{0.83}CuO_2$ has been reinvestigated and characterized by synchrotron diffraction experiments at high-temperature conditions. We noticed that the incommensurate modulated structure undergoes a structural transition beyond 540 K. The intrinsic composite nature of the compound is particularly evident by observing the apparently independent evolution of the Ca and CuO_2 sub-structures upon the temperature increasing. The Ca-sublattice undergoes a progressive contraction of the volume mainly related to the adjustment of the Ca-Ca distances alongside the a vector. The crystal structure stable at high temperature is featured by a diverse displacive modulation for of O1 and O2 defining relaxed octahedral sites if compared to the RT condition. The modulation vector q = 0.8510(5)c* + 0.013(4)a* yields to a new compositional variant approaching the a_{CuO2}/a_{Ca} = 0.851 ($6a_{Ca} = 7a_{CuO2}$ in first approximation) lattice relationship. The progressive recombination of the two sub-structures forming Ca_xCuO_2 outlines the unique structural versatility of composite crystals in combining competing structural factors in the same phase. Such structural results suggest forthcoming investigations from RT to 1000 K to explore the physical and chemical properties characterizing the high-temperature phase. In this frame, we are setting in-situ diffraction experiments on composite $Ca_{0.83}CuO_2$ dealing with the dynamical up-taking of NOx gases in the 500–700 K temperature range.

Supplementary Materials: The following are available online at http://www.mdpi.com/2073-4352/10/7/630/s1 High temperature evolution of the incommensurate composite crystal $Ca_{0.83}CuO_2$/s1, Figure S1: A collection of ED patterns of Ca_xCuO_2 compound. Figure S2: Rietveld plot obtained from the structural refinement of the (3D+1)-dimensional structure of composite crystal $Ca_{0.83}CuO_2$., Figure S3: Synchrotron diffraction patterns collected from 320K to 950K. Figure S4: Rietveld plot obtained from the structural refinement of the Ca-based composite crystal collected at 890K. Table S1: Refined amplitudes of the Fourier expansion associated to each atomic positions in the $Ca_{0.83}CuO_2$ (3D+1)-dimensional structure. Table S2: Crystal data for the monoclinic commensurate model of $Ca_5Cu_6O_{12}$. Table S3. Crystal data for the triclinic commensurate model of $Ca_6Cu_7O_{14}$ obtained at 890K.

Author Contributions: The synthesis of the ceramic compounds was undertaken by L.R. The synchrotron diffraction experiment has been conducted by L.R., M.M. and M.G.; methodology, M.M.; analysis of the diffraction data L.R.; data treatment of the synchrotron diffraction data, M.M.; writing—original draft preparation, L.R.; writing—review and editing, L.R. and M.G. All authors have read and agreed to the published version of the manuscript.

Funding: This research received no external funding

Acknowledgments: The authors are grateful to C. Dionigi and P. Nozar for the fruitful indications related to the synthesis of the $Ca_{0.83}CuO_2$ samples. We also thank A. Migliori for the assistance provided during the TEM investigations.

Conflicts of Interest: The authors declare no conflict of interest.

References

1. Brese, N.E.; O'Keeffe, M.; Von Dreele, R.B.; Young, V.G., Jr. Crystal structures of $NaCuO_2$ and $KCuO_2$ by neutron diffraction. *Solid State Chem.* **1989**, *83*, 1–7. [CrossRef]
2. Siegrist, T.; Roth, R.S.; Rawn, C.J.; Ritter, J.J. $Ca_{1-x}CuO_2$ $NaCuO_2$-type related structure. *Chem. Mat.* **1990**, *2*, 192–194. [CrossRef]
3. Pickardt, J.; Paulus, W.; Schmalz, M.; Schollhorn, R. Crystal-growth and structure refinement of $NaCuO_2$ by x-ray and neutron diffraction. *Solid. State Chem.* **1990**, *89*, 308–314. [CrossRef]
4. Choudhury, D.; Rivero, P.; Meyers, D.; Liu, X.; Cao, Y.; Middey, S.; Whitaker, M.J.; BarrazaLopez, S.; Freeland, J.W.; Greenblatt, M.; et al. Anomalous charge and negative-charge-transfer insulating state in cuprate chain compound $KCuO_2$. *Phys. Rev. B* **2015**, *92*, 201108. [CrossRef]
5. Karpinski, J.; Schwer, H.; Meijer, G.I. High-oxygen-pressure synthesis, structure and properties of the infinite-chain compound $Sr_{0.73}CuO_2$. *Phys. C Supercond.* **1997**, *274*, 99–106. [CrossRef]
6. Migliori, A.; Gemmi, M.; Calestani, G.; Belletti, D.; Matacotta, F.C.; Dionigi, C.; Nozar, P. Structure determination by electron diffraction and HREM of the incommensurate modulated phase Ba_xCuO_2 ($0.67 < x < 0.70$). *Phys. C Supercond.* **1999**, *328*, 89–103.
7. Karpinski, J.; Meijer, G.I.; Schwer, H.; Molinski, R.; Kopnin, E.; Angst, M.; Wisniewski, A.; Puzniak, R.; Hofer, J.; Rossel, C. High-pressure synthesis, crystal growth, phase diagrams, structural and magnetic properties of $Y_2Ba_4Cu_nO_{2n+x}$, $HgBa_2Ca_{n-1}Cu_nO_{2n+2+\delta}$ and quasi-one-dimensional cuprates. *New Dev. High. Temp. Supercond.* **2000**, *545*, 45–64. [CrossRef]
8. Meijer, G.I.; Rossel, C.; Henggler, W.; Keller, L.; Fauth, F.; Karpinski, J.; Schwer, H.; Kopnin, E.M.; Wachter, P.; Black, R.C.; et al. Long-range antiferromagnetic order in quasi-one-dimensional $Ca_{0.3}CuO_2$ and $Sr_{0.73}CuO_2$. *Phys. Rev. B* **1998**, *58*, 14452–14455. [CrossRef]
9. Van Smaalen, S.; Dinnebier, R.; Sofin, M.; Jansen, M. Structures of incommensurate and commensurate composite crystals Na_xCuO_2 (x = 1.58, 1.6, 1.62). *Acta Cryst. B* **2007**, *63*, 17–25. [CrossRef]
10. Duris, K.; Kremer, R.K.; Jansen, M. Synthesis, Crystal Structure, and Physical Properties of the New Chain Alkalioxocuprate $K_3Cu_2O_4$. *Zeitschrift fur Anorg. und Allgem. Chem.* **2011**, *637*, 1101–1107. [CrossRef]
11. Van Smaalen, S. Symmetry of composite crystals. *Phys. Rev. B* **1991**, *43*, 11330. [CrossRef]
12. Yamamoto, A. Unified setting and symbols of superspace groups for composite crystals. *Acta Cryst. A* **1992**, *48*, 476–481. [CrossRef]
13. Petricek, V.; Maly, K. The description and analysis of composite crystals. *Acta Cryst. A* **1991**, *47*, 210–216. [CrossRef]
14. Milat, O.; Van Tendeloo, G.; Amelinckx, S.; Babu, T.G.N.; Greaves, C. On the origin of the modulated structure in $Ca_{0.85}CuO_2$: An electron microscopy study. *Solid State Comm.* **1991**, *79*, 1059–1061. [CrossRef]
15. Milat, O.; Van Tendeloo, G.; Amelinckx, S.; Babu, T.G.N.; Greaves, C. Structural variants of $Ca_{0.85}CuO_2(Ca_{5+x}Cu_6O_{12})$. *Solid State Chem.* **1992**, *101*, 92–114. [CrossRef]
16. Miyazaki, Y.; Gamenson, I.; Edwards, P.P. A structural study of the quasi one-dimensional compound $(Ca_{1-x}Yx)_{(0.82)}CuO_2$ prepared at room pressure. *Solid State Chem.* **1999**, *145*, 511–516. [CrossRef]
17. Miyazaki, Y.; Onoda, M.; Edwards, P.P.; Shamoto, S.; Kajitani, T. Modulated structure of the composite crystal $Ca_{0.83}CuO_2$. *Solid State Chem.* **2002**, *163*, 540–545. [CrossRef]
18. Isobe, M.; Kimoto, K.; Muromachi, E. Structure and Magnetism of the Composite Crystal $Ca_{0.824}CuO_2$. *Low Temp. Phys.* **2003**, *131*, 737741.
19. Miyazaki, Y.; Huang, X.; Kajiwara, T.; Yamane, H.T.; Kajitani, T. Synthesis, crystal structure and physical properties of layered cobalt oxide Ca_xCoO_2 ($x \sim 0.47$). *Ceram. Soc. Jpn.* **2009**, *117*, 42–46. [CrossRef]
20. Foury-Leylekian, P.; Poltavets, V.V.; Jaouen, N.; Rueff, J.P.; Lorenzo, J.E.; Auban-Senzier, P.; Pasquier, C.R.; Mazzoli, C.; Greenblatt, M. Sodium ion and cobalt charge ordering in Na_xCoO_2 (x−5/6). *Phys. Rev. B* **2009**, *79*, 115101. [CrossRef]

21. Hiroi, Z.; Amelinckx, S.; VanTendeloo, G.; Kobayashi, N. Microscopic origin of dimerization in the CuO_2 chains in $Sr_{14}Cu_{24}O_{41}$. *Phys. Rev. B* **1996**, *54*, 15849–15855. [CrossRef]
22. Kataev, V.; Choi, K.Y.; Gruninger, M.; Ammerahl, U.; Buchner, B.; Freimuth, A.; Revcolevschi, A. Interplay of spin and charge dynamics in $Sr_{14-x}Ca_xCu_{24}O_{41}$. *Phys. Rev. B* **2001**, *64*, 104422. [CrossRef]
23. Hiroi, Z.; Azuma, M.; Takano, T.; Bando, Y. A new homologous series $Sr_{n-1}Cu_{n+1}O_{2n}$ found in the SrO CuO system treated under high pressure. *Solid State Chem.* **1991**, *95*, 230–238. [CrossRef]
24. Dolisek, J.; Arcon, D.; Cevc, P.; Milat, O.; Miljiak, M.; Aviani, A. Spin-dimer-like magnetic coupling in the infinite-chain compound $Ca_{0.85}CuO_2$. *Phys. Rev. B* **1998**, *57*, 7798. [CrossRef]
25. Isobe, M.; Kimoto, K.; Takayama-Muromachi, E. Spin-hole order in the 1-D chain cuprate $Ca_{0.824}CuO_2$. *Phys. B* **2003**, *329*, 1012–1013. [CrossRef]
26. Matsuda, M.J.; Garlea, V.O.; Ito, T.H.; Yamaguci, K.; Hozoi, L.; Rosner, H.; Schumann, R.; Kuzian, R.O.; Nishimoto, S. Highly dispersive magnons with spin-gap like features in the frustrated ferromagnetic S = 1/2 chain compound $Ca_2Y_2Cu_5O_{10}$ detected by inelastic neutron scattering. *Phys. Rev. B* **2019**, *100*, 104415. [CrossRef]
27. Cremona, A.; Fornasari, G.; Livi, M.; Petrini, G.; Trifirò, F.; Vaccari, A.; Vogna, E. Removal NOx from Lean Exhaust Gas by Absorption on Oxi-Anionic Materials. *Catal. Lett.* **2008**, *125*, 386–391. [CrossRef]
28. Arai, H.; Machida, M. Removal of NOx through sorption-desorption cycles over metal oxides and zeolites. *Catal. Today* **1994**, *22*, 97–109. [CrossRef]
29. Mosaddegh, E.; Hassankhani, A. Preparation, characterization, and catalytic activity of Ca_2CuO_3/$CaCu_2O_3$/CaO nanocomposite as a novel and bio-derived mixed metal oxide catalyst in the green synthesis of 2H-indazolo[2,1−b]phthalazine-triones. *Catal. Comm.* **2015**, *71*, 65–69. [CrossRef]
30. Petricek, V.; Dusek, M.; Palatinus, L.Z. Crystallographic computing system JANA2006: General features. *Zeits. Für Krist.* **2014**, *229*, 345–352.
31. Lambert, S.; Grebille, D. A 4D Composite Description for $Ca_{0.82}(Cu_{0.65}Co_{0.35}O_2)$. *Chem. Mater.* **2002**, *14*, 4904–4909. [CrossRef]
32. Qin, X.M.; Mai, W.J.; Li, J.M.; Li, F.Y.; Jin, C.Q. Fabrication and stability of the $Ca_{1-x}CuO_2$ chain structure during high-pressure and high-temperature sintering. *Alloy. Comp.* **2010**, *491*, 517–521. [CrossRef]